Generation and Stability of Toroidal Droplets in a Viscous Liquid

E. Pairam and A. Fernández-Nieves

School of Physics, Georgia Institute of Technology, Atlanta, Georgia 30332-0430, USA

(Received 4 February 2009; published 10 June 2009)

We use a simple method to generate toroidal droplets and study how they transform into spherical droplets. The method relies on the viscous forces exerted by a rotating continuous phase over a liquid which is extruded from an injection needle; the resultant jet is forced to close into a torus due to the imposed rotation. Once formed, the torus transforms into single or multiple spheres. Interestingly, we find there are two routes for this process depending on the aspect ratio of the torus. For thin tori, classical hydrodynamic instabilities induce its breakup into a precise number of droplets. By contrast, for sufficiently fat tori, unstable modes are unable to grow, and the torus evolves through a different route; it shrinks towards its center to coalesce onto itself, to finally form a single spherical droplet.

DOI: 10.1103/PhysRevLett.102.234501 PACS numbers: 47.20.Dr, 47.55.db, 47.55.Iv

Bubbles and droplets are common to our everyday life. They make rain and clouds and are essential constituents of many of the health care and food products we often use and eat. Bubbles and droplets are indeed ubiquitous in nature, and they have a spherical shape. Surface tension gives them their perfect spherical shape by minimizing the surface area for a given volume [1]. As a result, any means of dispersing a gas or a liquid in a fluid inevitably results in spherical bubbles or droplets. By contrast, generating fluid objects with nonminimal surface shapes, such as a torus, is far more complicated and still remains a formidable challenge. Despite the difficulty, this can be achieved by using external forces. For example, if rotated at sufficiently high speed, a freely suspended droplet can exhibit a variety of nonspherical shapes, including the torus; Plateau showed this experimentally [2] although it was not until about a century later that his observations were understood [3] and refined [4]. A bubble can also adopt the shape of a torus if vibrated [5] and dolphins make fascinating vortex rings, which have a toroidal shape [6,7]. Further examples are provided by the free fall of a droplet in an immiscible fluid [8,9] or by the impact of a droplet with a superhydrophobic surface [10]. Inevitably, the toroidal fluid generated by any of these means is unstable and always transforms into a spherical fluid once the external force vanishes. However, the details of this collapse are not known, reflecting in large measure the experimental difficulties in generating toroidal droplets under well-controlled conditions.

In this Letter, we report on a novel procedure to generate toroidal droplets and on how they transform into spherical droplets. Our technique enables precise control of the aspect ratio of the torus, which is in turn the relevant parameter determining its stability. For thin tori, the classical hydrodynamic instability causing the breakup of a long fluid cylinder, or jet, is also responsible for the breakup of the torus. In this case, however, only modes with a wavelength commensurate with the torus length can grow. Interestingly, for sufficiently fat tori, no unstable modes can develop, and the torus shrinks towards its center to finally coalesce onto itself. This shrinkage is always present irrespective of the aspect ratio of the torus, but becomes the dominant mechanism for sufficiently fat tori. Our results provide a simple way to make these unusual droplets and elucidate the way they transform, driven by surface tension, to the lowest energy spherical shape.

We inject a liquid through a metallic needle into a rotating bath containing a viscous continuous phase. As a result of the viscous drag exerted by the outer fluid over the extruded liquid, a curved jet forms at the exit of the needle, as shown in Fig. 1(a). However, if the rotational velocity, v_o, is not large enough, the jet breaks before the torus can be formed, as shown in Fig. 1(b). This suggests that the relevant time scales for the formation of a torus with our technique are the breakup time of the jet [11], $t_b \approx \eta_o a_{\mathrm{tip}}/\gamma$, with a_{tip} the inner radius of the needle, η_o the viscosity of the outer liquid, and γ the interfacial tension, and the time required to perform a full rotation, $T = 2\pi/\omega = 2\pi R_{\mathrm{tip}}/v_o$, with R_{tip} the distance from the needle to the rotation axis and $\omega = v_o/R_{\mathrm{tip}}$ the angular speed. By balancing these two time scales, we obtain the velocity needed to form a torus, $v_o = 2\pi(R_{\mathrm{tip}}/a_{\mathrm{tip}})(\gamma/\eta_o)$, which we can recast in terms of a capillary number: $\mathrm{Ca}_o \equiv \eta_o v_o/\gamma \approx 2\pi R_{\mathrm{tip}}/a_{\mathrm{tip}}$. This expression provides a means to predict whether a torus would form using our experimental method. To test its validity, we vary R_{tip} and v_o for different values of η_o and visually identify when a torus is formed. We summarize our observations in terms of Ca_o and $R_{\mathrm{tip}}/a_{\mathrm{tip}}$, as shown in Fig. 1(d). The line in this plot separates regions where a torus forms from regions where it does not form; it passes through the origin and has a slope of 5.5, which is close to 2π, consistent with our expectations.

Our method provides great flexibility in tuning the aspect ratio of the torus. On the one hand, its initial overall size, which we quantify by its initial overall radius, R_0, schematically shown in Fig. 1(c), is determined by the position of the injection needle with respect to the rotation

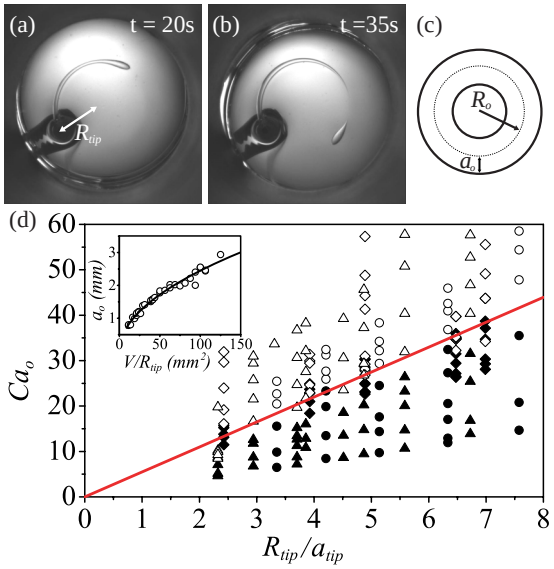

FIG. 1 (color online). (a) Formation and (b) breakup of a curved jet. In this experiment, the rotation speed is insufficient and the torus does not form. Instead, the jet breaks up before the torus is generated. (c) Geometrical parameters of a torus: Tube radius, a_0, and overall radius, R_0. (d) Diagram for the formation of toroidal droplets in terms of the capillary number of the outer liquid, Ca_o, and $R_{\mathrm{tip}}/a_{\mathrm{tip}}$, where R_{tip} is the distance between the needle and the rotation axis and a_{tip} is the inner radius of the needle. The different symbols correspond to different values of η_o: (◇, ◆) 30000 cP, (○, ●) 10 000 cP, (△, ▲) 5000 cP. The line corresponds to $\mathrm{Ca}_o = 5.5R_{\mathrm{tip}}/a_{\mathrm{tip}}$ and separates regions where the torus forms (open symbols) or does not form (closed symbols). We use water for the inner liquid and silicone oil for the outer liquid and always add the surfactant sodium dodecyl sulphate above its critical micelle concentration to decrease the interfacial tension to $\gamma = 4$ mN/m [22].

axis; as a result, $R_0 = R_{\mathrm{tip}}$. On the other hand, the injection flow rate and injection time determine the volume of the torus and thus the initial dimension of its tube, a_0. To show this, we made a series of tori all with $R_0 = 8$ mm, for different injection times, t_i, while keeping the injection flow rate equal to $q_i = 50$ ml/hr; in this way, we change the infused volume, $V = q_i t_i$. We obtain that a_0 increases with V/R_0, as shown in the inset of Fig. 1(d); this dependence quantitatively agrees with what would be expected for a torus, whose volume is equal to $V = 2\pi^2 a_0^2 R_0$, as shown by the line in the same figure. Thus, our method also provides a simple means to precisely vary the aspect ratio of the torus, R_0/a_0, by independently changing R_0 and a_0.

After the toroidal droplet is formed, we remove the needle and allow the system to evolve in time while recording the evolution with a CCD camera. For a viscosity ratio of the inner to the outer liquid of $\eta_i/\eta_o = 1/30$, we observe that the torus breaks into a precise number of droplets; this number depends on its initial aspect ratio, as shown by the series of images in Fig. 2, where we show snapshots for a wide range of R_0/a_0. The first row of images corresponds to the initial state, right after the needle is removed, the second row of images corresponds to a time slightly before breakup, and the third row of images corresponds to the end of the process, right after breakup had occurred. We obtain the same number of droplets for a well-defined range of aspect ratios, implying that the number of breakup points in the torus, n, as a function of R_0/a_0 is a step function, as shown in Fig. 3; each step is associated with a certain range of aspect ratios, all for the same n.

The observed breakup into a specific and discrete set of droplets implies that only wavelengths which are integer fractions of the overall length of the torus can induce its breakup. Consequently,

$$2\pi R_0 = n\lambda \tag{1}$$

with λ the wavelength associated to the mode inducing the breakup. Controlling R_0/a_0 thus provides a means to control the number of wavelengths that fit inside the torus, and, consequently, it allows us to control the number of droplets that result from its breakup.

Interestingly, we observe that the torus often shrinks before it breaks up into drops. For a given initial aspect ratio, the overall radius of the torus decreases until breakup occurs; this explains the presence of steps in Fig. 3. Furthermore, we observe that the torus breaks when the aspect ratio reaches the leftmost point of the step. For

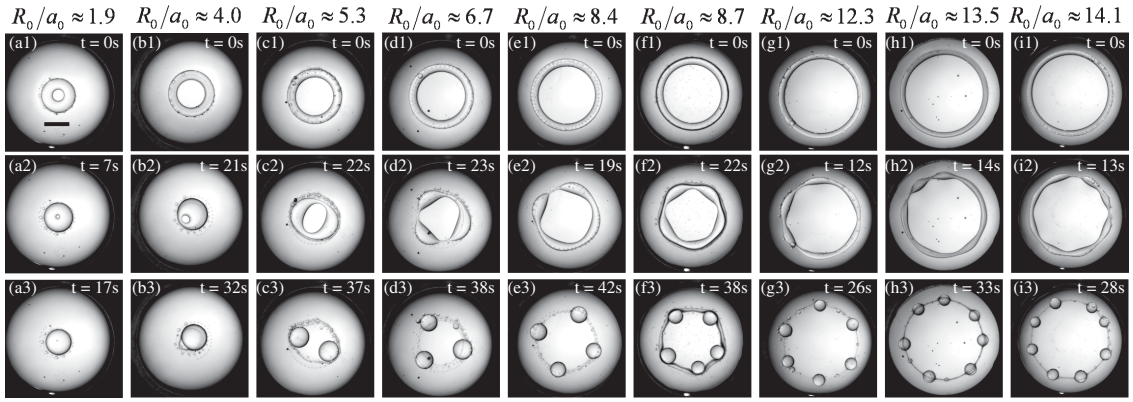

FIG. 2. Snapshots for the time evolution of a torus (from top to bottom) for different aspect ratios. The scale bar in (a1) corresponds to 5 mm. In these experiments, the injected liquid is glycerin and the liquid in the continuous phase is silicone oil ($\eta_i/\eta_o = 1/30$).

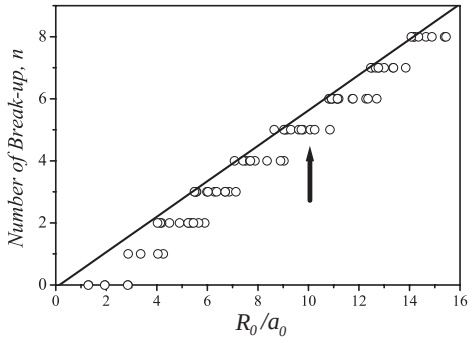

FIG. 3. Number of breakup points in the torus, n, as a function of its initial aspect ratio, R_0/a_0. The line corresponds to a linear fit of the leftmost points in the steps. We obtain $n \approx 0.57 R_0/a_0$.

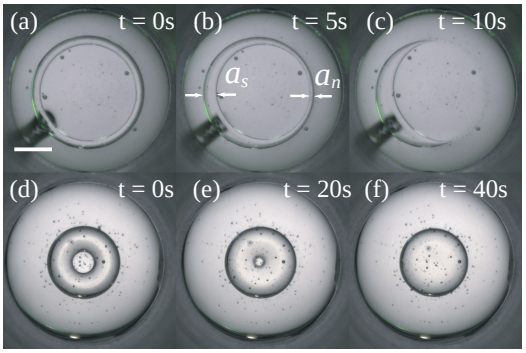

FIG. 4 (color online). Time evolution of a torus made of water immersed in silicone oil ($\eta_i/\eta_o = 1/30\,000$, $\gamma = 4$ mN/m). (a)–(c) Breakup of the torus through classical hydrodynamic instabilities. (d)–(f) Shrinkage and coalescence behavior for aspect ratios $R_0/a_0 \lesssim 2$. The scale bar corresponds to 5 mm.

example, a torus with an aspect ratio of ~10 (see arrow in Fig. 3) shrinks until the aspect ratio becomes ~8.3 corresponding to the leftmost point in the step; at this point, the torus breaks. Based on this observation, we hypothesize that when the torus reaches the leftmost point of each step, the mode inducing the observed n breakup corresponds to the mode with the largest growth rate possible; among all unstable modes, there is one which is the fastest [12], and we believe it is this mode that is responsible for the breakup. Based on this hypothesis, a torus will shrink until n wavelengths of this fastest mode can fit in the available contour length. As a result, irrespective of the aspect ratio, it is always the same mode that causes the breakup of the torus, with the only difference being the number of wavelengths that can fit in its contour length. Consistent with this hypothesis, the leftmost points of each step in Fig. 3 scale linearly with the aspect ratio, as shown by the linear fit in the same figure. We obtain that $n \approx 0.57 R_0/a_0$, which we can rewrite as $(n/R_0)a_0 = (2\pi/\lambda)a_0 \approx 0.57$ using Eq. (1); this provides the wavelength of the fastest unstable mode in our experiments. Remarkably, the classical stability analysis of Tomotika for a viscous, cylindrical jet inside another viscous liquid [13] predicts that the unstable mode with largest growth rate corresponds to $(2\pi/\lambda)a_0 = 0.54$ for $\eta_i/\eta_o = 1/30$; this value agrees with our experimental results, confirming our hypothesis.

We note, however, that for low aspect ratios, n can actually be equal to zero; there is no breakup in these cases, implying that the torus simply shrinks to coalesce onto itself, as shown in Fig. 2 (a1-a3). To inquire about this shrinking process, we recall that for fluid cylinders such that $\eta_i/\eta_o \to 0$ or $\eta_i/\eta_o \to \infty$, the unstable mode with the largest growth rate corresponds to $\lambda \to \infty$ [13]. This implies that only breakups with small n are expected in these situations. Consistent with this expectation, we only see breakups with $n = 1$ for a low viscosity ratio, $\eta_i/\eta_o = 1/30\,000$, as shown in Figs. 4(a)–4(c). In this case, there is only a single wavelength growing in the torus, and it corresponds to the fastest unstable mode that can grow.

Imposing a high viscosity ratio between the outer and inner liquid is thus ideal to explore what happens for small n. We perform a series of experiments with tori of varying aspect ratio and monitor the time evolution of the tube radius both where it is largest (swell), a_s, and where it is smallest (neck), a_n, normalized by the initial tube radius, as shown in Fig. 5(a). For large aspect ratios, we find that a_s grows with time while a_n decreases with time; these behaviors are symmetric with respect to the initial state, $a_s = a_n = a_0$. If a_n decreases, a_s must increase, since the volume of the torus is conserved. Interestingly, for smaller aspect ratios, this symmetrical behavior is not retained. In these cases, the torus appreciably shrinks with time, as shown in Fig. 5(b), where we plot the inner radius of the torus, $R_{\rm in}(t)$, schematically shown as an inset, normalized with the initial inner radius, as a function of time. We observe that the torus shrinks towards the center irrespective of the aspect ratio. However, this shrinkage is more important as R_0/a_0 decreases, thus causing the asymmetric behavior of a_n and a_s with respect to a_0; the observed

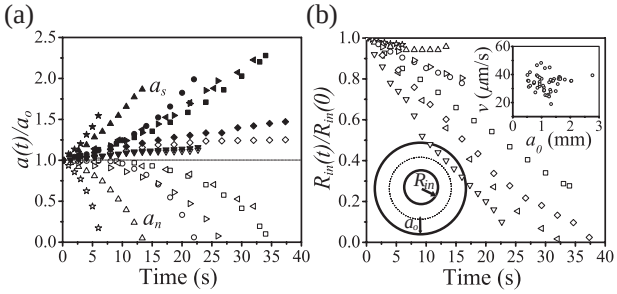

FIG. 5. (a) Time evolution of the swell (closed symbols) and neck (open symbols) radii normalized with the initial radius, for different values of the aspect ratio: (★, ☆) $R_0/a_0 \approx 11.1$, (▲, △) $R_0/a_0 \approx 5.6$, (●, ○) $R_0/a_0 \approx 3.6$, (▶, ▷) $R_0/a_0 \approx 2.6$, (■, □) $R_0/a_0 \approx 2.2$, (◀, ◁) $R_0/a_0 \approx 2.1$, (◆, ◇) $R_0/a_0 \approx 1.9$, (▼, ▽) $R_0/a_0 \approx 1.4$. (b) Time evolution of the torus dimension, quantified through $R_{\rm in}(t)$ normalized with $R_{\rm in}(0)$, for different values of the aspect ratio [symbols as in (a)]. Inset: Initial velocity of the shrinkage process as a function of a_0. The velocity is independent of a_0 and equal to (34 ± 6) μm/s. In all these experiments, $\eta_i/\eta_o = 1/30\,000$ and $\gamma = 4$ mN/m. The schematic shows a torus with $R_{\rm in} \approx a_0$.

shrinkage enhances the growth of a_s while diminishes the decrease of a_n, which eventually even increases with time.

In fact, for $R_0/a_0 \lesssim 2$, there is no breakup, and the torus relies on the shrinkage mechanism in order to transform into a single spherical droplet; the torus simply shrinks towards its center to coalesce onto itself, as shown in Figs. 4(d)–4(f) for $\eta_i/\eta_o = 1/30\,000$. As a result, there is no neck anywhere along the contour of the torus and both a_s and a_n increase with time, as shown in Fig. 5(a). Interestingly, the condition $R_0 \approx 2a_0$ corresponds to a torus having a tube radius equal to R_{in}, as shown in the schematic of Fig. 5(b). Based on this measure, the contour length of such torus would be $2\pi R_{\text{in}} \simeq 2\pi a_0$. This condition is reminiscent of the classical limit of Plateau and Rayleigh [14,15] separating stable and unstable modes in a linear tube; only those modes with a wavelength larger than $2\pi a_0$ are unstable. We emphasize, however, that the connection between our experiments and this classical result only holds if R_{in} is taken as the relevant dimension: When $R_{\text{in}} \lesssim a_0$, we find that no unstable mode grows in the torus, which simply shrinks to finally form a single spherical droplet.

To quantify this shrinkage behavior, we measure the initial speed, v, of the process and plot the result as a function of a_0 in the inset of Fig. 5(b). We observe that the speed of the shrinkage process does not appreciably depend on a_0. Instead, the speed is constant and equal to (34 ± 6) μm/s. To account for this value, we balance the two relevant forces in the process: Surface tension, which provides the driving force, and a viscous drag per unit length, which opposes the shrinkage process. We estimate the drag on our tori by considering the drag on a cylinder [16], $F/L = 4\pi\eta_o v/\ln(7.4/\text{Re})$, where $\text{Re} = \rho v a_0/\eta_o$ is the Reynolds number and L is the length of the cylinder. From the condition $F/L \approx \gamma$, we get $v = 140$ μm/s, which is a factor of $\sim$4 larger than the experimental result [17]. In addition, since the drag only depends on a_0 through the logarithm of Re^{-1} and $\text{Re} \approx O(10^{-6})$, v should not depend on a_0, consistent with our experimental observations.

Our results provide insight on how a toroidal droplet transforms into a spherical droplet suggesting an interesting interplay between the two relevant length scales in the problem, the radius of the contour length, R_0, and the radius of its circular cross section, a_0. The classical hydrodynamic breakup competes with a shrinkage mechanism in order to induce the transition to the energetically favored spherical shape. For thin tori, classical hydrodynamic instabilities induce breakup, while for fat tori, only the shrinkage mechanism can exist causing the subsequent shape transformation. We hope that our simple interpretations provide the starting point for more detailed hydrodynamic calculations; among other things, we believe these calculations should implicitly consider the curvature of the torus, as well as the time dependent character of λ, which results from its shrinkage.

We also emphasize that our results rely on a novel and simple method to generate toroidal droplets of precise aspect ratio, which could serve as a basis to make toroidal objects for a wide range of studies, for example, to analyze geometrical frustration in the curved space of a torus [18]. Additionally, as with spherical droplets, which have inspired insight into a wide range of systems, including the atomic nucleus [19], our toroidal droplets might also serve as a model for other physical systems. An important issue still to be resolved pertains to the overall stability of the torus; a possible direction in this respect might include the use of complex fluids, such as colloidal suspensions [20,21].

We acknowledge very insightful conversations with R. Grigoriev, H. A. Stone, and J. M. Gordillo. We thank H. A. Stone, R. Grigoriev, P. Segre, and A. Zangwill for reading the manuscript. We also thank DPI2008-06624-C03-03.

[1] C. V. Boys, *Soap Bubbles—Their Colours and the Forces which Mould Them* (Dover Publication, New York, 1959).
[2] J. Plateau, *Statique Experimentale et Theorique des Liquides Soumix aux Seules Forces Moleculaires* (Gauthier-Villars, Paris, 1873).
[3] R. A. Brown and L. E. Scriven, Proc. R. Soc. A **371**, 331 (1980).
[4] R. J. A. Hill and L. Eaves, Phys. Rev. Lett. **101**, 234501 (2008).
[5] F. Zoueshtiagh *et al.*, Eur. Phys. J. E **20**, 317 (2006).
[6] J. K. Walters and J. F. Davidson, J. Fluid Mech. **17**, 321 (1963).
[7] T. J. Pedley, J. Fluid Mech. **32**, 97 (1968).
[8] N. Baumann *et al.*, Phys. Fluids A **4**, 567 (1992).
[9] M. C. Sostarecz and A. Belmonte, J. Fluid Mech. **497**, 235 (2003).
[10] Y. Renardy *et al.*, J. Fluid Mech. **484**, 69 (2003).
[11] To estimate this time scale, we balance the driving force due to surface tension with the viscous force, which is the relevant opposing force in our experiments: $\gamma \approx \eta_o v = \eta_o a_{\text{tip}}/t_b$, where $v = a_{\text{tip}}/t_b$ is a representative velocity for the pinching process of a jet of radius $a_{\text{jet}} \approx a_{\text{tip}}$.
[12] S. Chandrasekhar, *Hydrodynamic and Hydromagnetic Stability* (Oxford University Press, New York, 1961).
[13] S. Tomotika, Proc. R. Soc. A **150**, 322 (1935).
[14] J. Plateau, Acad. Sci. Bruxelles Mem. **23**, 5 (1849).
[15] L. Rayleigh, Proc. R. Soc. London **29**, 71 (1879).
[16] G. K. Batchelor, *An Introduction to Fluid Dynamics* (Cambridge University Press, New York, 2000).
[17] We emphasize that this force balance is only intended to provide an order of magnitude estimate for the speed. More precise calculations considering the intrinsic curvature of the torus and the flow field around it, which must certainly differ from that around a cylinder, would be required to further develop this rough estimate.
[18] L. Giomi and M. J. Bowick, Phys. Rev. E **78**, 010601(R) (2008).
[19] N. Bohr and J. A. Wheeler, Phys. Rev. **56**, 426 (1939).
[20] A. B. Subramaniam *et al.*, Nature (London) **438**, 930 (2005).
[21] O. D. Velev, A. M. Lenhoff, and E. W. Kaler, Science **287**, 2240 (2000).
[22] A. S. Utada, A. Fernández-Nieves, H. A. Stone, and D. A. Weitz, Phys. Rev. Lett. **99**, 094502 (2007).